

ZnFe₂O₄: Rapid and sub-100 °C synthesis and anneal-tuned magnetic properties†Ranjit Sai,^{ab} Suresh D. Kulkarni,^{ab} K. J. Vinoy,^c Navakanta Bhat^{ac} and S. A. Shivashankar^{*ab}

Received 29th September 2011, Accepted 2nd November 2011

DOI: 10.1039/c1jm14874e

Nanocrystalline zinc ferrite (ZFO) has been synthesized from metal acetylacetonates by microwave irradiation for 5 min in the presence of a surfactant. The as-prepared material is ZFO and has been subjected in air to conventional furnace annealing and to rapid annealing at different temperatures. Both annealing protocols lead to well-crystallized ZFO, with crystallite sizes in the range ~8–20 nm, which is ferrimagnetic, even at room temperature, with magnetization attaining saturation. While the magnetization M_S of conventionally annealed ZFO varies with crystallite size in the expected manner, rapid annealing leads to high M_S even when the crystallite size is relatively large. The coercivity is greater in the conventionally annealed ZFO. Thermal and magnetic measurements suggest that the inhomogeneous site cationic distribution within each crystallite caused by rapid annealing can be used to tailor the magnetic behaviour of nanocrystalline ferrites.

Introduction

There has been renewed effort in the synthesis of spinel ferrites in recent years, prompted by reports of novel properties of these oxides in the nanometric regime. The effort is spurred also by the miniaturization of magnetic and electronic devices, which demands advanced materials that have smaller sizes, new forms, and shapes. Hence there are many recent reports on nanoparticles of different ferrites, which have traditionally been prepared in the bulk.¹ Specifically, nanoparticles of zinc ferrite (ZnFe₂O₄ or ZFO) have generated a lot of interest because of their potential applications in gas sensing,^{2,3} semiconductor photocatalysis,⁴ as the magnetic core of RF devices⁵ and in magnetic resonance imaging.⁶

Ferrites with normal and inverse spinel structures exhibit a variety of magnetic ordering and properties, depending on the choice of the ion for the tetrahedral A-site. In zinc ferrite, ZnFe₂O₄ (ZFO), a normal spinel, with nonmagnetic Zn²⁺ ions on tetrahedral sites only, magnetic interaction takes place only between the Fe³⁺ ions, which occupy only the octahedral B sites. As such, bulk ZnFe₂O₄, a normal spinel, displays antiferromagnetic ordering below 10 K, and short range ordering at higher temperatures.^{7–9} However, it has been shown recently that, as the average particle size is reduced, ZFO exhibits

ferrimagnetic behaviour. As various studies have shown,^{2,3,10–12} this is because of the distribution of both Zn²⁺ and Fe³⁺ among the A and B sites of the “partially inverted” spinel lattice whereas, in “bulk” ZFO, Zn²⁺ and Fe³⁺ occupy only the A and B sites, respectively. The degree of such inversion, and the resulting changes in the magnetic properties of ZFO, have been found to depend sensitively on the method of synthesis and the subsequent (thermal) processing of the nanocrystalline material.^{3,4,8,9,13–19}

Complex oxides like ZnFe₂O₄ may be synthesized by different techniques, such as sol–gel,²⁰ combustion,²¹ coprecipitation,²² microemulsion,²³ polyol,¹⁴ normal and reverse micelle,¹³ sonochemical,^{18,19} *etc.*, apart from traditional ceramic synthesis processes.¹⁶ The latter involve physical mixing of the individual oxides (or oxide precursors, such as carbonates and oxalates), calcinations, sintering at high temperature for extended durations, grinding and, finally, re-sintering. These processes require long reaction times and rather high temperatures that are undesirable both from technological and environmental points of view. Furthermore, traditional ceramic synthesis routes do not provide control of the grain size or a narrow size distribution at the nanometric level. Therefore, sol–gel synthesis has been employed in recent years. However, the inherent disadvantages of the sol–gel method are the formation of multiphase materials and the lengthy processing required. The disadvantages of the combustion synthesis and spray pyrolysis techniques are their rather large “thermal budget”, the non-uniformity of the crystallite size they entail, and the need for safety requirements.²¹ On the other hand, the hydrothermal process is one of the most promising methods for preparing fine ceramic powders.^{15,24} A microwave-assisted hydrothermal synthesis of ceramics was first attempted by Komarneni *et al.*²⁵ The main advantages of microwaves-based process over the conventional hydrothermal

^aCentre for Nano Science and Engineering, Indian Institute of Science, Bangalore, India

^bMaterials Research Centre, Indian Institute of Science, Bangalore, India. E-mail: shivu@mrc.iisc.ernet.in; Tel: +91-8022932782

^cElectrical Communication Engineering, Indian Institute of Science, Bangalore, India

† Electronic supplementary information (ESI) available. See DOI: 10.1039/c1jm14874e

process are that the kinetics of the reaction are enhanced manifold, thus reducing process time, and that novel phases can be obtained by the method. Microwave irradiation, a contactless process, produces efficient and high rates of heating of a sample (in the form of a solution for the present context) at the molecular level, leading to a uniform increase in temperature, and to high yields and reproducibility.²⁶

Specifically, Komarneni *et al.*²⁵ used the microwave-hydrothermal method to prepare nano-sized powders of various ferrites with high specific surface areas. They reported using a closed-vessel system, irradiated with microwaves at 2.45 GHz and ~650 W of power, to synthesize ferrites from aqueous solutions of metal hydroxides. Crystalline ferrites were formed within 4 min of reaction time at 100 psi and 164 °C, at a yield >80%. However, traces of haematite (α -Fe₂O₃) were also formed. Subsequently, Jin-Ho Lee *et al.*²⁷ attempted to optimize the reaction conditions (pH, temperature, and time) for the same process, seeking to obtain the pure ferrite. It was found that a 30-min-long exposure to microwaves at the higher temperature of 180 °C eliminates the variations due to the pH of the solution. However, neither of these two studies reported the magnetic properties of the material synthesized by the microwave hydrothermal method.

Most of the magnetic studies reported on nanocrystalline ZFO to date have involved material processed over long durations, effectively yielding equilibrium compositions of the resulting ZFO. Microwave-assisted synthesis in the solution medium, by contrast, is relatively rapid, which is likely to influence the occupancy of the A and B sites in the resulting nanocrystalline ZFO, and thereby its magnetic behavior. If, in addition, the post-synthesis treatment of nanocrystalline ZFO is carried out by rapid thermal annealing, the magnetic (and other) properties of ZFO would be characterized by the site occupancies induced by such rapid processing.

The aim of the present effort has been to develop a pH-independent recipe for the preparation of ZnFe₂O₄ nanoparticles by microwave-assisted synthesis in the solution medium, followed by thermal treatment that seeks to alter the resulting ZFO. We thus report a rapid, microwave-assisted, soft-chemical technique for the *in situ* synthesis of phase-pure nanocrystalline ZnFe₂O₄, its subsequent thermal treatment by two different protocols, and the characterization of the resulting oxide. The magnetic properties of ZFO so obtained are also reported. We show that microwave-assisted synthesis is an efficient and rapid process for the preparation of ferrimagnetic nanocrystals at low temperature.

Experimental

We have employed safe, common solvents and metal-organic precursors, namely metal acetylacetonates,²⁸ which possess low moisture sensitivity and are thus less susceptible to hydrolysis, rendering them superior to metal alkoxides and halides often used in oxide synthesis. The metal-oxygen bond present in acetylacetonate complexes makes them appropriate precursors for the synthesis of oxides.

The metal complexes, Fe(III)acetylacetonate (Fe(acac)₃), and Zn(II)acetylacetonate (Zn(acac)₂), were synthesized and purified in-house.^{29,30} The AR-grade solvents and the surfactant, cetyl

trimethylammonium bromide (CTAB), were used as received. The typical procedure employed for the synthesis of nanoparticles of ZFO by the microwave-assisted chemical process is as follows. Solutions of 1 mmol of Zn(acac)₂ and 2 mmol of Fe(acac)₃ in 25 ml and 50 ml of ethanol, respectively, were mixed and transferred to a 250 ml round-bottomed (RB) flask, while 0.4 g of CTAB dissolved in 25 ml of water was added to it. This reaction mixture was irradiated in a “domestic” microwave oven (2.45 GHz, 800 W, 5 min), fitted with a water-cooled reflux condenser to avoid the loss of solvent during the reaction. A brown precipitate was formed upon allowing it to cool to room temperature. The schematic diagram of the apparatus (Fig. 1) also illustrates the optical fiber temperature sensor directly in contact with the solution for accurate measurement of reaction temperature. The solid precipitate was separated by centrifugation (10 min at 4000 rpm), and washed repeatedly with ethanol and acetone to remove unreacted material, and dried in air.

The powder precipitates were subjected to heat treatment in air at different temperatures under two different protocols (Table 1). In the first, conventional annealing (CA) [ramp rate: 10 °C min⁻¹] was carried out in a muffle furnace for a chosen duration; in the second, annealing was performed in a home-made rapid annealing (RA) apparatus [ramp rate: 200 °C min⁻¹] for a chosen duration (see the ESI†). Labels in Table 1 indicate the temperature and duration of annealing. It is expected that, for a very short duration, the samples RA32 and RA52 attain a temperature considerably higher than indicated in Table 1, because of the high intensity of the halogen lamps as they are turned on, and because of the loose thermal anchoring of the powder sample to the silicon substrate on which it was placed.

A thermal study of the as-prepared powder was carried out in air over the temperature range of 25–900 °C using a simultaneous thermo-gravimetric/differential thermal analyzer (TG/DTA, TA

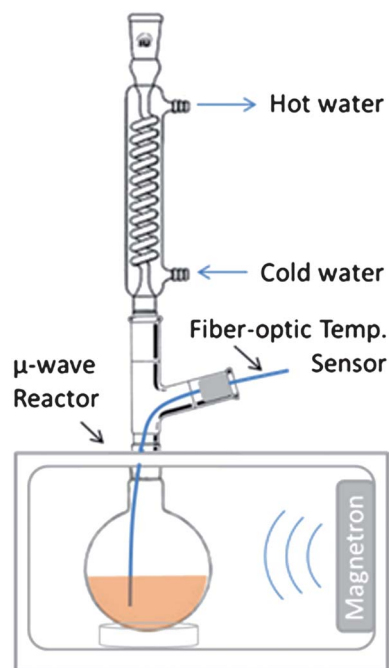


Fig. 1 Schematic diagram of the modified domestic microwave oven used for the synthesis of ZFO.

Table 1 ZFO samples and their post process treatment

Sample name	Anneal protocol	Ramp-up rate	Ramp-down rate
UA00	As-prepared	—	—
CA32	CA [2 h @ 300 °C]	10 °C min ⁻¹	5 °C min ⁻¹
RA32	RA [2 min @ 300 °C]	200 °C min ⁻¹	150 °C min ⁻¹
CA52	CA [2 h @ 500 °C]	10 °C min ⁻¹	5 °C min ⁻¹
RA52	RA [2 min @ 500 °C]	200 °C min ⁻¹	150 °C min ⁻¹

instruments, SDTQ-600). Thermogravimetric analysis of the as-prepared powder was also carried out in the isothermal mode, in air, so as to mimic the conditions of CA and RA. In mimicking CA, as-prepared ZFO is heated (at 20 °C min⁻¹) in air to 300 °C, where it is held for 2 h, further heating followed (at 20 °C min⁻¹) up to 500 °C, and held again for 2 h. Similarly for RA, the as-prepared sample was heated in air rapidly (at 80 °C min⁻¹) to 300 °C (nominal) and held there for 2 min, heated further at the same rate to 500 °C (nominal), and held there for 2 min. Elemental analysis (CHNS) of the powder material was performed (Thermo Finnigan FLASH EA 1112 analyzer). The crystallinity of samples and their phase composition were examined by X-ray powder diffractometry (XRD, JEOL JDX-80300), using Cu-K α radiation. Transmission electron microscopy (TEM, TECNAI F-30, 200 kV) was employed to perform electron diffraction, and to determine particle sizes and the particle size distribution. Magnetic measurements on the powder samples were made using a SQUID magnetometer (Quantum Design MPMS XL-5).

Results and discussion

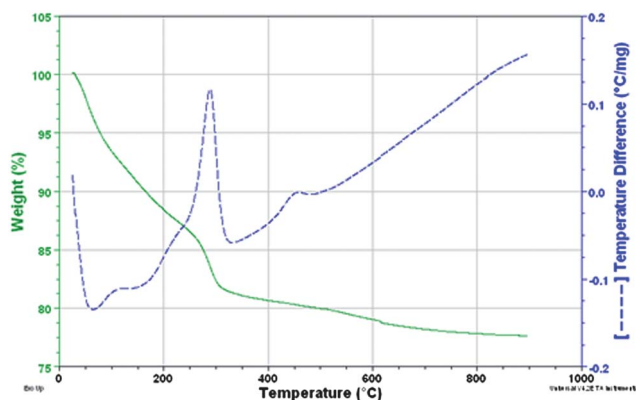
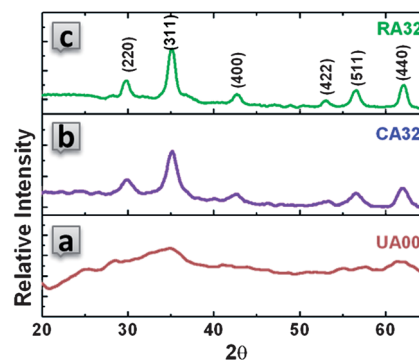
Under microwave irradiation, the temperature of the reaction mixture is found not to exceed 95 °C (see the ESI†). It is therefore possible that organic moieties are a part of the powder precipitate. To examine this and to determine the minimum temperature required (in air) to remove them, TG/DTA data were gathered on the as-synthesized sample from room temperature to 900 °C (Fig. 2).

One broad endothermic peak and one strong exothermic peak are present in the DTA data up to 300 °C, accounting together for a total weight loss of 18%. This weight loss and the associated thermal events may be attributed to desorption of solvents and the combustion of organic moieties from the metal complexes

and the surfactant (CTAB). Another broad exothermic event takes place between 400 °C and 500 °C (Fig. 2). To understand it, elemental analysis was carried out on the CA32 and CA52 samples, which revealed that their total organic content (by weight) was 3.7% and 1.1%, respectively. Thus, thermal and elemental analyses together show that the weight loss (2.6%) between 300 °C and 500 °C is due to the removal of organic moieties and, therefore, that annealing the as-prepared powder at ~300 °C would suffice to remove most of the organic chemical moieties.

XRD patterns of the as-prepared and annealed samples are shown in Fig. 3 and Fig. 4. The as-prepared sample (UA00, Fig. 3a) shows broad peaks, characteristic of very small crystals, whereas all the annealed samples (Fig. 3b, 3c and 4) feature distinct sharpening of the diffraction peaks of UA00, corresponding to improved crystallinity (grain growth). The diffraction patterns can be indexed to cubic zinc ferrite, ZnFe₂O₄ (PCPDF No. 82-1049) and no other crystalline phase detected. Given these findings, the weight loss of 2.4% between 500 °C and 900 °C (Fig. 2) can be attributed to loss of oxygen from the lattice.

TEM analysis was used to study on a fine scale the morphologies of the various powder samples and to obtain particle size distribution data. The selective area electron diffraction (SAED) pattern for the as-prepared powder shown in Fig. 5(a) reveals diffuse rings characteristic of disordered or barely crystalline material. However, the SAED patterns for the annealed samples (Fig. 5b–e) show rings with spots, characteristic of well-crystallized (polycrystalline) material; the patterns are assignable to cubic ZnFe₂O₄. No other crystalline phase is present in these SAED patterns, attesting to the phase purity of the oxide obtained by the microwave method, followed by annealing (CA/RA). The lattice parameter of the annealed

**Fig. 2** Simultaneous TGA/DTA of the as-prepared ZFO.**Fig. 3** XRD patterns of the (a) as-prepared and (b) & (c) annealed ZFO samples.

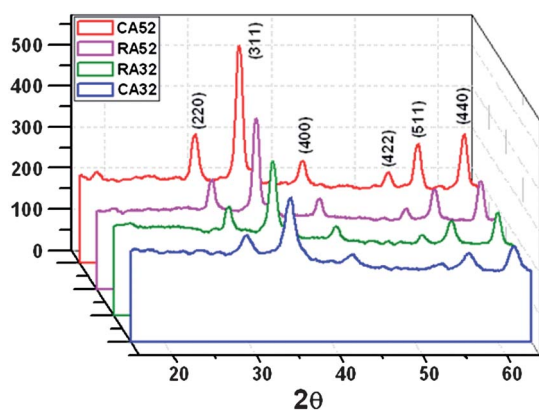


Fig. 4 XRD patterns of various annealed ZFO samples.

samples was calculated from the SAED patterns and found to be $8.45 \pm 0.01 \text{ \AA}$, in good agreement with the value reported for bulk zinc ferrite (8.44 \AA). While the sample CA32 comprises very fine crystals, the crystallites in the other annealed samples display clearly polyhedral shapes characteristic of cubic symmetry, indicating that even a brief exposure to elevated temperatures, as in RA32 and RA52, suffices to allow grain growth and the attainment of equilibrium shapes (Fig. 6). The individual particles appear to be single-crystalline, as shown by lattice imaging (Fig. 5f). Grain size distribution within the annealed samples was found to be narrow and Gaussian (Fig. 5), as estimated by counting ~ 200 nanocrystals. The average crystallite sizes are given in Table 2.

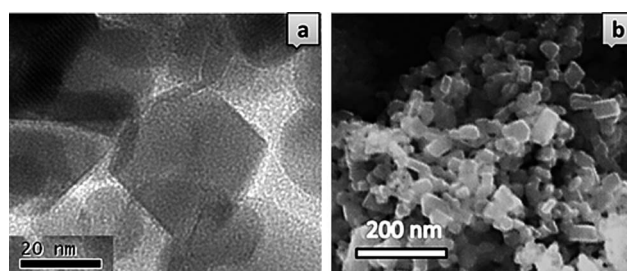


Fig. 6 (a) TEM and (b) SEM images of sample RA32 show vividly that even rapid annealing suffices for the formation of equilibrium shapes of ZFO.

Magnetic properties

The magnetic properties of a nanocrystalline ferrite, such as ZnFe_2O_4 , depend inherently on the cationic distribution in the lattice. As already noted, zinc ferrite in nanometric size is a partly inverse spinel, with the Zn^{2+} and Fe^{3+} cations occupying both A and B sites in the lattice. The degree of inversion increases as the particle size is reduced, and is largely dependent on the method of preparation.¹¹ As magnetic properties of ZFO are determined by crystallite size and the degree of inversion, even within the same composition, the two different annealing protocols used are an attempt to alter the degree of inversion.

As-prepared ZFO

The saturation magnetization (M_S) and coercivity (H_C) of the various samples, measured on a SQUID magnetometer, are

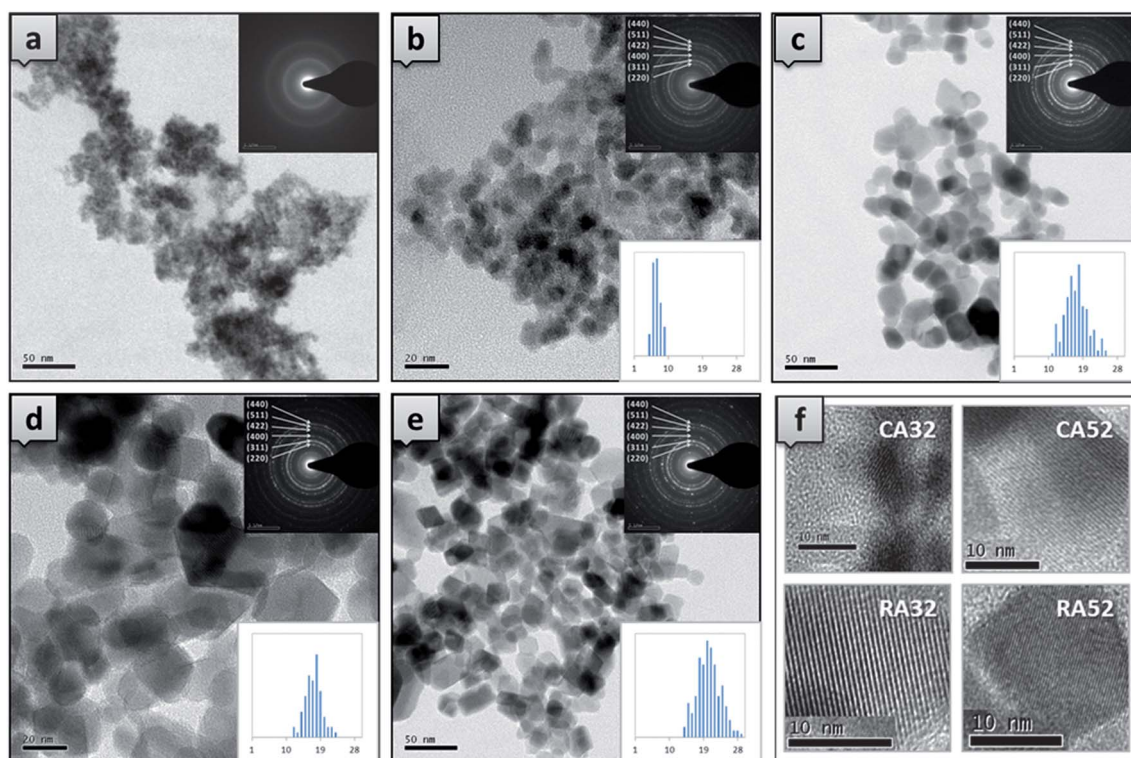


Fig. 5 TEM images and analysis of ZFO samples (a) UA00 (b) CA32 (c) CA52 (d) RA32 (e) RA52. (f) HRTEM images of the annealed samples. The SAED patterns and the histograms track the growth of crystallites due to annealing on the 1–30 nm scale.

Table 2 Crystallite size and magnetic parameters of ZFO samples

Sample name	Crystallite size/nm	M_S @ 30 K/emu g ⁻¹	H_C @ 30 K/Oe	M_S @ 300 K/emu g ⁻¹	H_C @ 300 K/Oe
UA00	— ^a	12.50	18	2.6	0
CA32	8.4	39.41	20	7.93	5
RA32	17.5	38.75	50	7.50	28
CA52	18.1	26.98	198	6.62	12
RA52	20.8	33.19	65	5.55	38

^a Due to agglomeration and very small sizes (<5 nm) a precise value is not shown.

given in Table 2. The hysteresis (M – H) curve (Fig. 7a) of the as-prepared ZFO (UA00) displays: (i) superparamagnetism at 300 K, with zero coercivity (Fig. 7b); and (ii) ferrimagnetism at 30 K, even though the coercivity is only 5 Oe and the saturation magnetization is ~ 12.5 emu g⁻¹. As seen from XRD data (Fig. 3a), the crystallites in the as-prepared sample (UA00) are very small (<5 nm). Nevertheless, the material displays saturation in magnetization, unlike nanocrystalline ZFO prepared by other methods.^{11,31} It is to be noted here that microwave irradiation-assisted synthesis not only features a low process temperature, but also a high degree of nucleation in the medium of growth (the solution), limiting the size of the crystallites as formed. Furthermore, the higher rate of crystallite growth in the present process, than in other low temperature processes for nanomaterial synthesis, may be expected to influence site occupancy by metal ions (degree of inversion) to be different from that in the thermodynamically most stable configuration in bulk ferrite,⁸ and in nanocrystalline ZFO prepared by slower methods. Thus, the observed saturation magnetization M_S and measurable coercivity (at 30 K) in the as-prepared sample may be attributed to the cationic distribution among the A and B sites resulting from microwave synthesis.

On the other hand, saturation magnetization of the as-prepared ferrite (UA00), even at 30 K, is low, which may be attributed to the very small size of the crystals, with a large fraction of their atoms residing on the surface. In nanocrystalline magnetic materials, there is disorder among the surface spins, arising from dangling bonds of the surface atoms, leading to greater anisotropy and weak magnetization.¹¹ Such disorder has been reported in other spinel ferrites as well.^{32–34}

Annealing vs. magnetic behaviour

During post-synthesis annealing, the fine crystallites of the ferrite in the as-prepared material begin to coalesce and grow. Two hours of annealing at 300 °C (CA32) leads to crystallites of 8.4 nm, with a significantly higher (than in UA00) M_S of 39.4 emu g⁻¹ at 30 K (Fig. 8a). Similar annealing at 500 °C (CA52) leads to larger crystallites (18.1 nm), but a lower saturation magnetization, *i.e.*, 27.0 emu g⁻¹ at 30 K (Fig. 8a). The trend is the same when measurements are made at 300 K (Fig. 8d). This trend may be understood by noting that, during lengthy conventional annealing (CA32, CA52), the ferrite crystallites grow larger, whereby the contribution from surface spin disorder is reduced. The crystals still being nanometric, the partial inversion present leads to a higher value of M_S than in UA00, in which the crystals are much smaller. However, in CA52, the higher annealing temperature not only leads to crystallite growth, but also to cationic redistribution towards that in normal-spinel ZFO. This explains¹⁴ the smaller value of M_S in CA52 than in CA32.

By contrast, two minutes of rapid annealing nominally at 300 °C (RA32) leads to crystallites of 17.5 nm, which are ferrimagnetic, with M_S of 38.7 emu g⁻¹ at 30 K (Fig. 8a), while a similar rapid anneal nominally at 500 °C (RA52) leads to larger crystallites (21 nm), with a somewhat lower M_S of 33.2 emu g⁻¹ at 30 K. Rapid annealing is known to promote rapid grain growth and possibly introduce defects. However, being by definition a brief process RA may be expected not to affect the cation site occupancy^{8,35} significantly. The difference in M_S between samples annealed at low and high temperature is greater in CA than in RA, regardless of whether M_S is measured at 30 K or 300 K (Fig. 8a and 8d). The trends in the variation of magnetization with crystallite size for the two annealing protocols are shown

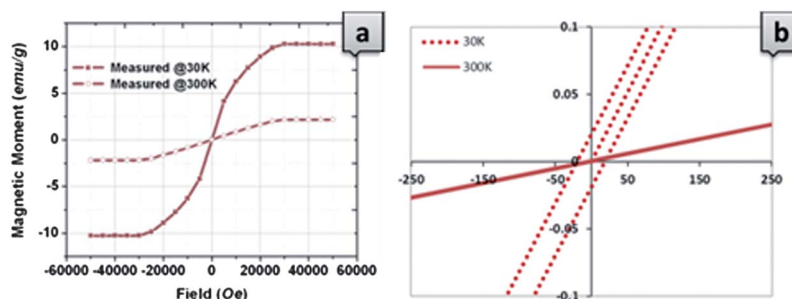


Fig. 7 M – H curves of ZFO sample (UA00) measured at 30 K and 300 K: (a) full scale; (b) at expanded field-strength scale.

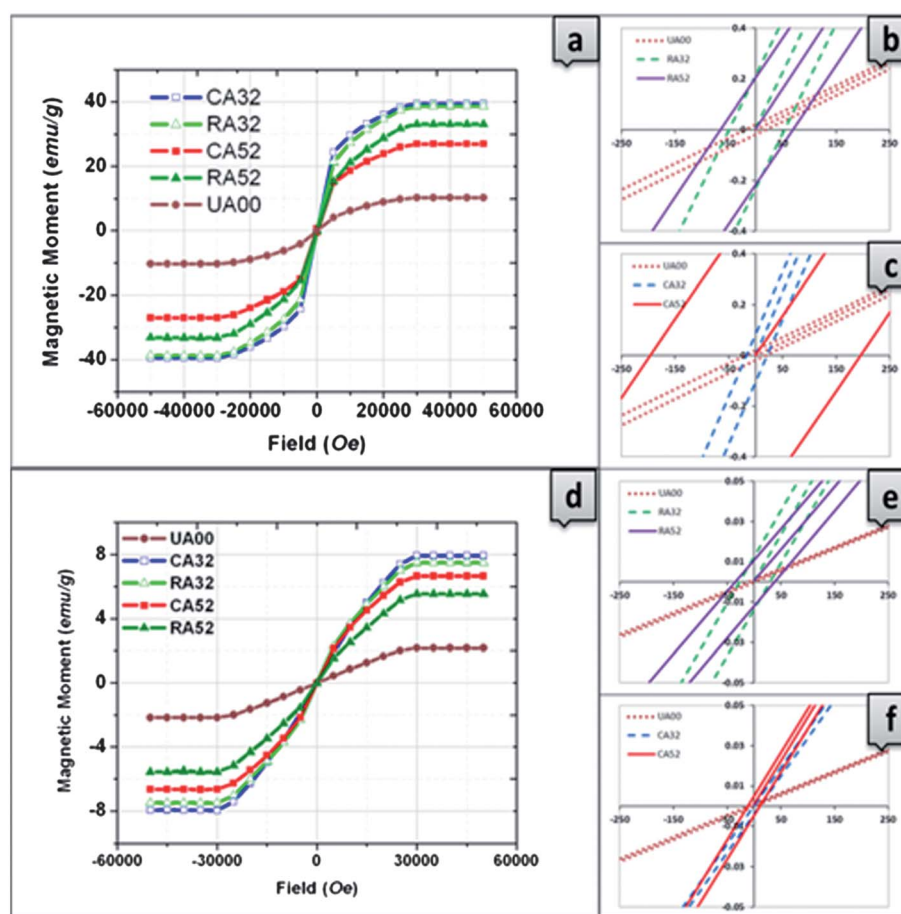


Fig. 8 M - H curves of annealed ZFO samples (a) measured at 30 K; (b) expanded M - H curves of UA00, RA32 and RA52 at 30 K; (c) expanded M - H curves of UA00, CA32 and CA52 at 30 K, (d) measured at 300 K; (e) expanded M - H curves of UA00, RA32 and RA52 at 300 K; (f) expanded M - H curves of UA00, CA32 and CA52 at 300 K.

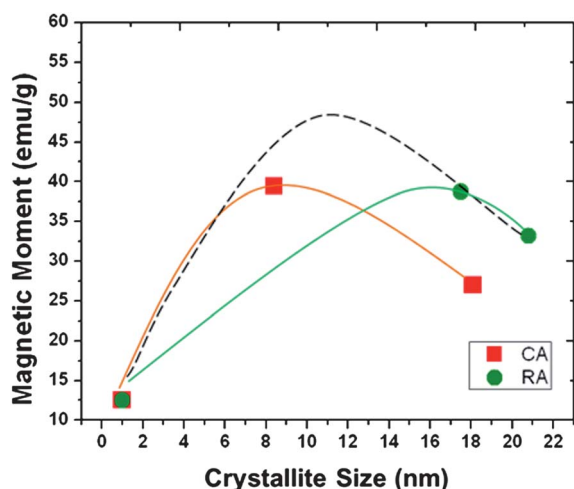


Fig. 9 Variation of M_S with crystallite size in CA and RA samples. The dotted curve projects the possible optimization of M_S by “tuning” the RA process.

schematically in Fig. 9, and are found to be similar but of different magnitudes. An earlier report¹¹ shows that M_S increases as the crystallite size decreases, but only up to a limiting size,

below which M_S decreases with any further reduction in crystallite size.

Though M_S vs. crystallite size shows the same trend in CA and RA, the actual magnetization depends on the annealing scheme. A closer look at the data in Fig. 9 and Table 2 reveals that, at 30 K, (i) M_S is the highest in CA32, in which the average particle size is the smallest, consistent with other reports on ZFO. However, M_S is nearly as high in RA32, though the particle is twice as large. By contrast, (ii) M_S is smaller in CA52, even though the particle is comparable to RA32, while (iii) RA52, despite its marginally larger particle size, has a larger M_S than CA52. These observations are in contrast with previous reports,^{14,22,24} where a consistent relationship between M_S and crystallite size is reported. The present results show that, in nanoferrites, not only the process of synthesis, but also the annealing protocol alters the structure/composition and, thereby, magnetic behaviour. That is, the M_S of nanoferrites depend on various parameters, *viz.*, degree of inversion, surface disorder, and anisotropy, each of which is affected by processing.

Isothermal TGA of the CA and RA samples reveals the different ways in which they are affected by the two protocols (Fig. 10a, 10b). The weight loss due to CA at 300 °C is negligible, while it is 0.98% at 500 °C. By contrast, the weight loss due to RA at 500 °C is much smaller (0.08%). As these samples have first

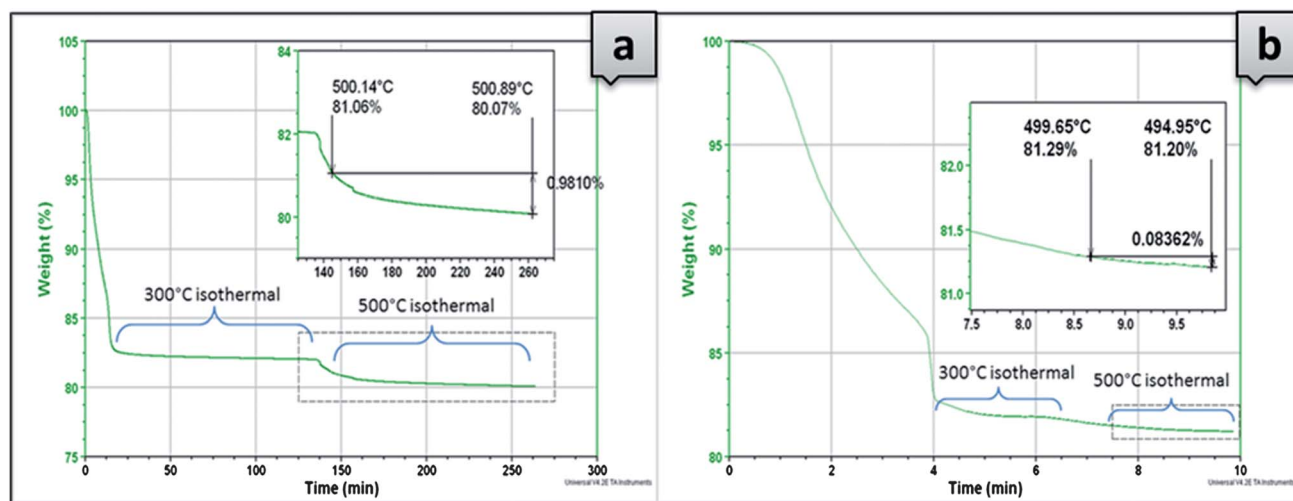


Fig. 10 Isothermal TGA data for the as prepared ZFO samples held for: (a) two hours at 300 and 500 °C each imitating the CA process; (b) two minutes at 300 and 500 °C (nominal) each imitating the RA process. Both (a) and (b) show an expected large weight loss during the temperature ramp-up.

been annealed under CA and RA protocols (and thus the organic content has been removed), the above weight losses are attributable to the loss of oxygen from the ferrites. Hence, the degree of inversion in the CA and RA samples can be expected to be different. In particular, the rapidity of the RA process limits oxygen loss, and is likely to result in the inhomogeneity of oxygen content (and thus the degree of inversion) within a given crystallite.

These various factors affect not only M_S but also the coercivity of the annealed samples, both at 30 K and 300 K. It is to be noted (Table 2) that the highest coercivity at 30 K is measured in CA52, the sample which may be expected to be the closest to equilibrium structure and composition, including the degree of inversion, because of the prolonged treatment at 500 °C. The equally long annealing at 300 °C of the sample CA32 is not likely to have been as effective in attaining the corresponding equilibrium because of the slower kinetics at 300 °C. As is well known,³¹ H_C is influenced by the degree of inversion, crystallite size and, thus, by surface states. Given that CA52 represents equilibrium processing, inhomogeneity of inversion within crystallites is unlikely. Thus, it may be inferred that this homogeneity, and the larger crystallite size in CA52 that renders surface states less important, is conducive to attaining a larger H_C .

The small values of H_C at 30 K in the RA samples, despite their large values of M_S , indicate the relative importance of the various parameters in determining M_S and H_C , as measurement temperature is varied. That is, a high value of M_S does not necessarily result in high H_C . The low value of H_C at 30 K in the RA samples probably indicates the detrimental effect of inhomogeneous inversion on H_C , suggesting that crystalline and compositional perfection, and the effects of surface anisotropy, are more important in determining H_C at low temperature than at room temperature. At 300 K, H_C in RA32 and RA52 is considerably greater than in CA52, which displays the highest H_C at 30 K. This may be interpreted as the effect of “pinning” magnetic order that inhomogeneity in inversion has at high temperatures. Thermal effects appear to suppress H_C in the CA samples, which are otherwise more “perfect” than the RA

samples. In the RA samples, the adverse thermal effects on H_C are probably overwhelmed by the effects of “pinning”. Thus, it appears possible that rapid post-synthesis processing and microwave-assisted rapid chemical synthesis can be combined to tailor the microstructure and magnetic properties of nanocrystalline ZFO. It can be expected that, by optimizing the processing conditions, the value of M_S may be raised to a higher value than reported here, as projected in Fig. 9.

One salient feature of the annealed ZFO samples of the present effort is that they are ferrimagnetic up to room temperature, with a corresponding saturation magnetization (Fig. 8a and 8d). This contrasts with reports³¹ showing that saturation is not attained in nanocrystalline ZFO prepared from solution through “soft” methods, followed by prolonged annealing, presumably resulting in equilibrium structure and composition. Indeed, the present results are consistent with the rapid growth of high quality, crystalline nanostructures of ZnO from $\text{Zn}(\text{acac})_2$ through microwave irradiation, in the as-prepared form.³⁶ Reaction rate enhancement by microwaves is largely attributed to thermal effects involving microwave dielectric heating mechanism, wherein “molecular radiators” are formed through collisions between molecular moieties set rotating by the direct coupling of microwave energy and reagents.²⁶ As a result, locally high temperatures are generated, leading to rapid formation of products from the energized molecules.³⁷ In a typical synthesis of the present type (precursors in solution) chemical reactions generate “monomers” for nucleation which, in due course, undergo growth to produce nanocrystals. It is surmised that the very high density of nucleation that occurs instantly in the solution, upon irradiation, leads to nanocrystals of high quality, with equilibrium morphology attained either during synthesis itself or during grain growth that occurs *via* subsequent annealing, however brief. It is likely also that ZFO is partially inverted as-grown, consistent with the size of the nanocrystals that result from the high nucleation density. This is supported by the saturation of magnetization, and appreciable coercivity, measured in the as-grown sample (at 30 K).

Conclusions

Nanocrystalline zinc ferrite can be synthesized within minutes when a solution of metal acetylacetonates is irradiated with microwaves, in the presence of a surfactant. While the as-prepared material is superparamagnetic at room temperature, it is ferrimagnetic at low temperature. Conventional, prolonged furnace annealing in air leads to a well-crystallized ZFO that displays saturation magnetization, as well as an appreciable coercivity, both at room and low temperature. Rapid annealing for two minutes suffices to achieve significant grain growth and well-faceted crystallites, with M_S greater than in conventionally annealed ZFO, both at room and low temperature. While the variation of M_S with crystallite size in conventionally annealed ZFO is consistent with earlier reports, rapid annealing leads to site occupancy of metal ions in the ferrite lattice different from that in equilibrium (conventional) annealing. This results in significantly higher M_S for a given ZFO crystallite size than does conventional annealing. However, conventional annealing leads to greater coercivity at low temperature for a given crystallite size, although H_C is greater at room temperature in rapid-annealed ZFO. These findings show that rapid annealing causes inhomogeneity in cationic occupancy within crystallites, altering the magnetic properties of ZFO, suggesting that annealing protocols can be employed to tailor the magnetic behaviour of nanocrystalline ferrites.

Acknowledgements

The authors are grateful for financial support from the Dept. of Information Technology, Govt. of India and from the National Program on Micro and Smart Systems (NPMAS)

Notes and references

- G. Caruntu, G. G. Bush and C. J. O'Connor, *J. Mater. Chem.*, 2004, **14**, 2753.
- S. Zhuiykov, T. Ono, N. Yamazoe and N. Miura, *Solid State Ionics*, 2002, **152–153**, 801–807.
- C. Xiangfeng, L. Xiangqin and M. Guangyao, *Sens. Actuators, B*, 1999, **55**, 19–22.
- C. Wang, Y. Ao, P. Wang, J. Hou and J. Qian, *J. Hazard. Mater.*, 2010, **184**, 1–5.
- C. Yang, F. Liu, T. Ren, L. Liu, H. Feng, A. Z. Wang and H. Long, *Sens. Actuators, A*, 2006, **130–131**, 365–370.
- C. Bárcena, A. K. Sra, G. S. Chaubey, C. Khemtong, J. P. Liu and J. Gao, *Chem. Commun.*, 2008, 2224–6.
- K. Kamazawa, Y. Tsunoda, K. Odaka and K. Kohn, *J. Phys. Chem. Solids*, 1999, **60**, 1261–1264.
- C. Nordhei, A. L. Ramstad and D. G. Nicholson, *Phys. Chem. Chem. Phys.*, 2008, **10**, 1053–66.
- W. Schiessl, W. Potzel, H. Karzel, M. Steiner, G. Kalvius, a. Martin, M. Krause, I. Halevy, J. Gal, W. Schäfer, G. Will, M. Hillberg and R. Wäppling, *Phys. Rev. B: Condens. Matter*, 1996, **53**, 9143–9152.
- U. Steinike and K. Tkacova, *J. Mater. Synth. Process.*, 2000, **8**, 197–203.
- L. Tung, *Phys. B*, 2002, **319**, 116–121.
- M. A. Valenzuela, P. Bosch, J. Jiménez-becerrill, O. Quiroz and A. I. Páez, *J. Photochem. Photobiol., A*, 2002, **148**, 177–182.
- J. F. Hochepped, P. Bonville and M. P. Pileni, *J. Phys. Chem. B*, 2000, **104**, 905–912.
- S. Ammar, N. Jouini, F. Fiévet, Z. Beji, L. Smiri, P. Moliné, M. Danot and J.-M. Grenèche, *J. Phys.: Condens. Matter*, 2006, **18**, 9055–9069.
- M. Andrés Vergés, M. Martínez and E. Matijević, *J. Mater. Res.*, 1993, **8**, 2916–2920.
- G. F. Goya and H. R. Rechenberg, *J. Appl. Phys.*, 2000, **87**, 8005–8007.
- H. H. Hamdeh, J. C. Ho, S. A. Oliver, R. J. Willey, G. Oliveri, G. Busca and I. Introduction, *J. Appl. Phys.*, 1997, **81**, 1851–1857.
- E. K. Nyutu, W. C. Conner, S. M. Auerbach, C.-H. Chen and S. L. Suib, *J. Phys. Chem. C*, 2008, **112**, 1407–1414.
- M. Sivakumar, T. Takami, H. Ikuta, A. Towata, K. Yasui, T. Tuziuti, T. Kozuka, D. Bhattacharya and Y. Iida, *J. Phys. Chem. B*, 2006, **110**, 15234–43.
- M. Atif, S. Hasanain and M. Nadeem, *Solid State Commun.*, 2006, **138**, 416–421.
- K. C. Patil, M. S. Hegde, T. Rattan, and S. T. Aruna, *Chemistry of Nanocrystalline Oxide Materials*, World Scientific Publishing Co. Pte. Ltd., 2008.
- T. Kamiyama, K. Haneda, T. Sato, S. Ikeda and H. Asano, *Solid State Commun.*, 1992, **81**, 563–566.
- H. Zhu, X. Gu, D. Zuo, Z. Wang, N. Wang and K. Yao, *Nanotechnology*, 2008, **19**, 405503.
- C. Upadhyay, H. Verma, V. Sathe and A. V. Pimpale, *J. Magn. Magn. Mater.*, 2007, **312**, 271–279.
- S. Komarneni, M. C. D. Arrigo, C. Leonelli and G. C. Pellacani, *J. Am. Ceram. Soc.*, 1998, **81**, 3041–3043.
- I. Bilecka and M. Niederberger, *Nanoscale*, 2010, **2**, 1358.
- J. Lee, *J. Alloys Compd.*, 2001, **325**, 276–280.
- A. L. Willis, Z. Chen, J. He, Y. Zhu, N. J. Turro and S. O. Brien, *J. Nanomater.*, 2007, **2007**, 14858.
- H. A. Tayim and M. SabriVoi, *Inorg. Nucl. Chem. Lett.*, 1973, **9**, 753–757.
- G. Rudolph and M. C. Henry, *Inorg. Chem.*, 1964, **3**, 1317–1318.
- V. Blanco-Gutiérrez, M. J. Torralvo-Fernández and R. Sáez-Puche, *J. Phys. Chem. C*, 2010, **114**, 1789–1795.
- R. H. Kodama, A. E. Berkowitz, J. E. J. McNiff and S. Foner, *Phys. Rev. Lett.*, 1996, **77**, 394–397.
- M. Muroi, R. Street, P. G. McCormick and J. Amighian, *Phys. Rev. B: Condens. Matter*, 2001, **63**, 184414.
- N. Mouden and M. P. Pileni, *J. Phys. Chem.*, 1996, **100**, 1867–1873.
- J. Bernardi, *J. Magn. Magn. Mater.*, 2000, **219**, 186–198.
- S. Brahma, K. J. Rao and S. Shivashankar, *Bull. Mater. Sci.*, 2010, **33**, 89–95.
- L. Zhenyu, X. Guangliang and Z. Yalin, *Nanoscale Res. Lett.*, 2006, **2**, 40–43.